2010 American Control Conference
Marriott Waterfront, Baltimore, MD, USA
June 30-July 02, 2010

An Electric Ray Inspired Biomimetic Autonomous Underwater Vehicle

P. Krishnamurthy, F. Khorrami, J. de Leeuw, M. E. Porter, K. Livingston, J. H. Long, Jr.

Abstract— **The development of a novel Biologically-inspired (or Biomimetic) Autonomous Underwater Vehicle (BAUV) inspired by the Pacific electric ray is addressed. The design and hardware implementation of experimental prototypes of the "RayBot" BAUV are described. Extensive observations of live electric rays provided key biological inspirations in the development of the BAUV. As part of the effort, a six degree-of-freedom impulse-based multi-body approach for modeling and simulation of BAUVs was also developed and validated through comparison with experimental data.**

I. Introduction

Autonomous Underwater Vehicles (AUVs) have attracted increasing interest [1–3] in recent years due to their potential important role in several civilian and military applications such as intelligence and surveillance applications, search and rescue, mobile communication relays, and hull and pier inspection with object identification and localization. The AUV system should also be efficient to minimize size, weight, and power (SWaP) requirements. A promising direction in which to seek innovative designs for AUVs with the aforementioned desirable characteristics is biology and the examination of the mechanisms used in natural swimmers. Hence, Biologically-inspired (or Biomimetic) Autonomous Underwater Vehicles (BAUVs), "artificial fish" in particular, are receiving significant attention [4,5] due to the attractive promise of being able to leverage optimizations achieved over millions of years of evolution. The biological study of real fishes and their swimming mechanisms [6,7] offers key design ideas to achieve energy efficiency, stealth, and maneuverability in BAUVs.

By virtue of 560 million years of natural selection, fish have evolved into more than 25,000 living species, each representing a composite of solutions to a particular ecological problem, from burrowing quickly in sediments to migrating hundreds of kilometers with low-power propulsors. The study of fish swimming mechanisms provides a large set of potential design ideas. Selecting an appropriate model from this set of potential design ideas depends critically on matching the engineering design inputs to the species that most closely embodies the desired solution. In this effort, an artificial fish design based on the biological model of the electric ray was explored and a self-propelled autonomous hardware prototype was engineered. The electric ray is a particularly well suited design target in this effort due to its high maneuverability, power efficiency, ability to work near the bottom, availability of a rigid body disk providing a stable platform for a payload, and relative mechanical simplicity. Unlike non-electric rays and skates, electric rays do not use their disk for thrust generation. Instead, the expanded caudal fin is oscillated by the muscular tail. They are also capable of bottom walking using the pectoral crus. Importantly, electric rays are built to carry a substantial payload, their electric organs, and this region of the disk is held rigid. Electric rays can cruise in midwater and operate in close proximity to the bottom. They are also very maneuverable, able to rotate in yaw about their center of mass.

The RayBot BAUV was designed based on efficiency, performance versatility, maneuverability, stealth, compactness, payload capacity, and cost considerations. The BAUV design draws upon qualitative and quantitative data collected experimentally from live and frozen rays as part of this effort (Section II). The effort included development of a BAUV multi-body based modeling framework and a simulation and visualization platform as described in Section III. The hardware implementation of experimental prototypes of the designed RayBot BAUV and experimental testing are presented in Section IV.

II. Biological Inspiration

The biological models used as inspiration in this work are electric rays (Figure 1), cartilaginous elasmobranch fish of the Order Torpediniformes [9], possessing a highly-specialized, dorsoventrally flattened circular disc evolved from the head, body, and pectoral fins of shark-like ancestors.

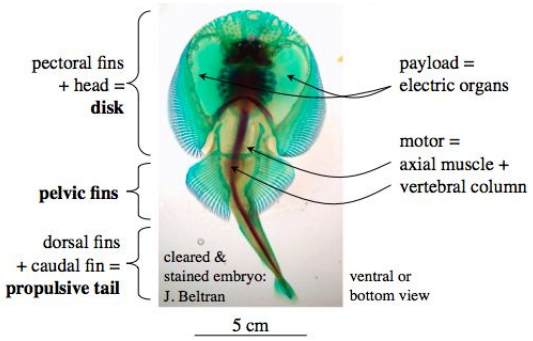

Fig. 1. Functional anatomy of electric ray.

Fig. 2. Live electric rays, mother and neonate, used for observation.

Electric rays make an excellent model (Figure 2) for the following reasons [10,11]:

- Their oscillatory tail is the only propulsor for swimming. Their disk is not used for thrust production, unlike morphologically-similar skates and sting rays, which oscillate or undulate their wing-like disc margins. This greatly simplifies the engineering of motor and control systems while taking advantage of the hydrodynamic and payload carrying advantages of the electric ray

The first two authors are with Control/Robotics Research Laboratory (CRRL), Department of Electrical and Computer Engineering, Polytechnic Institute of NYU, Brooklyn, NY, 11201. The second author is also with IntelliTech Microsystems, Inc. The third to sixth authors are with Vassar College, Poughkeepsie, NY, 12604. This work was supported in part by ONR under contract no. N00014-08-M-0293. Emails: pk@crrl.poly.edu, khorrami@smart.poly.edu, jodeleeuw@vassar.edu, meporter@vassar.edu, livingst@vassar.edu, jolong@vassar.edu.

configuration. Furthermore, they have a thin profile for low-drag propulsion.

- Their paired pelvic fins are shape-changing, specialized for non-propulsive control surfaces. They maneuver rapidly in yaw using the moment arm provided by their tail acting against the low resistance of their flattened disk. Because the disk is non-propulsive, they can hold their anterior body disk rigid, providing a stable payload platform. The electric ray is built to carry a large payload, the electric organ, i.e., arrays of electrocytes that deliver a prey-stunning shock.
- They are stealthy, burrowing themselves shallowly in sediments, leaving just the eyes visible; their flattened body disk has a low frontal profile, minimizing bow wave effects. They are multi-modal locomotors: they cruise using the oscillating tail which has high moment arm for maneuvering; the walk on the surface using pectoral crus or fin "legs"; they maneuver using disk, tail, and fins; they can also burrow.
- Their disk is a partially-flexible lifting body, with a perimeter skirt that can change shape and perhaps modulate lift-generating capabilities.
- They station-hold on the bottom passively using their body's negative buoyancy. They scale as free-swimmers from 10 cm to $>$ 1 m in length.

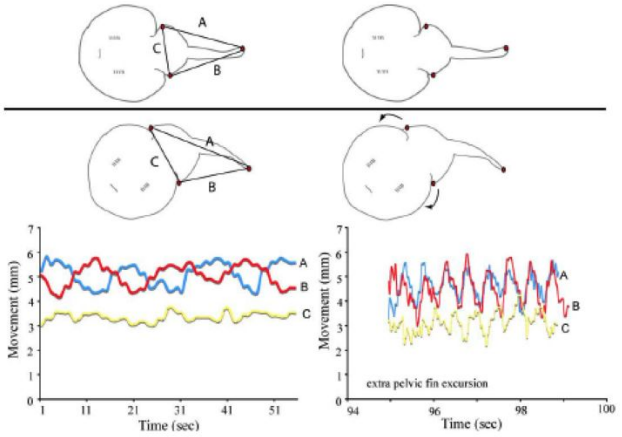

Fig. 3. Tailbeat kinematics of neonate electric rays: Two modes of steady swimming.

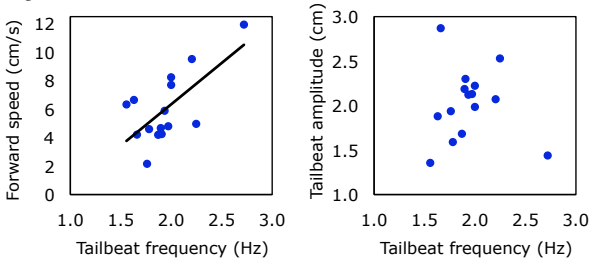

Fig. 4. Constant-velocity swimming kinematics of electric ray: blue dots are samples from observations of free-swimming juvenile electric rays (three months old), using a combination of mode 1 and mode 2 swimming. Black line in left figure is a linear fit of the observations.

The design of the RayBot BAUV draws upon qualitative and quantitative experimental observations from our laboratory adult and juvenile electric rays to provide design inputs for this effort. Extensive experimental data have been collected from the juveniles over a period of many months representing individuals ranging in size from 7 cm to 40 cm in total length. One goal of the data collection was to be able to document the ontogenetic changes in swimming performance that occur as these animals increase their size. Swimming trials were performed in a 3 m long, clear-bottomed tank with salt water and videotaped (30 Hz frame rate, HD video) simultaneously from the side and the bottom using a mirror angled at 45^o under the tank. We observed two modes (Figure 3) of steady forward swimming, previously undescribed in the scientific literature: mode 1, in which the rays held their pelvic fins steady relative to their bodies while the caudal fin and tail generate the propulsive force, and mode 2, in which the rays oscillated their pelvic fins in conjunction with their tails. Mode 2 is associated with faster swimming speeds. Mode 1 is similar to the swimming behavior of the adult electric ray. The two modes of swimming are illustrated in Figure 3. Mode 1 shown in the left column in Figure 3 is characterized by lateral caudal fin and tail undulations, shown as a change in the length of lines A and B, without a change in the width of the pelvic fins, C (and line C). Mode 2 (the right column in Figure 3) is characterized by the lateral motion of the tail and caudal fin as well as lateral movement of the pelvic fins (line C) wherein in addition to lateral undulations of the tail and caudal fin, the pelvic fins are moved in a cranial to caudal motion during the tailbeat. Pelvic fin movement is illustrated by the cyclical patterns of line C in the right panel of Figure 3.

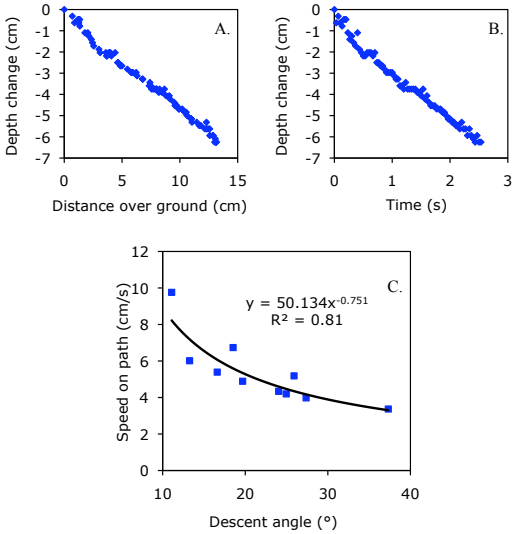

Fig. 5. Gliding behavior of electric ray: A and B. Depth change example in a free-swimming juvenile (three months old); C. Speed as a function of descent angle based on observations from ten trials, with power fit.

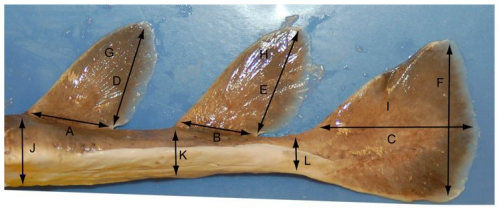

Fig. 6. Propulsive fins of electric ray. Three fins - first dorsal, second dorsal, and caudal - participate in propulsion by providing trailing edges for vortex shedding. Lines indicate measurements taken on four individuals averaging a body disk length of 15.8 cm and body width of 16.1 cm.

Steady forward swimming is modulated by tailbeat frequency; as tailbeat frequency increases, forward speed also increases (left figure in Figure 4). There is no significant relationship between tailbeat amplitude and frequency in swimming neonates (right figure in Figure 4). Speed along the glide path, without any propulsive movement from the caudal fin, is a function of the descent angle, measured as the

angle of the body relative to the horizontal (Figure 5). For the purpose of providing information about fin size, shape, and position on the body for our simulation and robot, we also measured the morphology of the dorsal and caudal fins on adult electric rays (Figure 6). The propulsive tails contain three fins, each with a trailing edge that will act, via the Kutta condition, as a trailing edge and vortex shedder.

III. Modeling and Simulation Platform

To analyze the swimming behavior of the electric ray and to provide guidance for the design of the RayBot, a simulation and visualization platform was implemented based on a multi-body approach [8]. Interest in understanding the swimming of fish [12,13] and, in recent years, in developing BAUVs has spurred research into various techniques for fish and BAUV modeling (for instance, [14–17] and references therein) using primarily approaches based on quasi-steady aerodynamic theory and starting from a focus on modeling of the swimming behavior restricted to single-direction forward swimming on to planar (two translational and one rotational degree of freedom) swimming and, in recent years, to three-dimensional swimming considering also diving (depth change) behavior. Modeling and simulation based on Computational Fluid Dynamics (CFD) approach has also been addressed (for instance, in [18] and references therein); however, a CFD approach is computationally burdensome and does not lend itself to development of a model usable for control design purposes. An impulse-based multi-body approach for BAUV modeling was proposed in [8] based on a formulation of a BAUV as the composition of a collection of bodies interlinked through appropriate joints. The hydrodynamic effects on each body are expressed through quasi-steady aerodynamic approximations and the dynamics of the entire BAUV system is attained through the utilization of a impulse-based approach [19,20] for capturing the effects of the joint constraints. This modeling approach is generally applicable to any BAUV with arbitrary arrangements of foils and addresses full six degree-of-freedom (6DOF) dynamics of the BAUV including roll and pitch motions. The dynamic modeling technique proposed in [8] is based on an articulated multi-body approach (Figure 7), which provides generality and flexibility in terms of support for various fin configurations and designs. Details on the dynamic modeling of biomimetic underwater vehicles was addressed in [8] and are omitted here for brevity. Compared to the conventional approach utilized in the robotic fish modeling and control literature wherein the dynamics of the multiple parts of the fish are not modeled explicitly and the cumulative external (hydrodynamic + gravity) force and torque are simply viewed as acting on a rigid body capturing the inertia properties of the entire BAUV, this approach offers improved fidelity. However, while this approach treats the different parts as hydrodynamically independent, it is to be noted that further fidelity improvements can be attained through a detailed flow modeling including cross-coupling between different parts. In the proposed approach, the parts of the BAUV that can move relative to each other are modeled as separate rigid bodies and the coupling between the parts is modeled in terms of constraints involving joints of various kinds (hinge, ball-and-socket, slider, etc.). Flexible parts such as the tail and flexible body used in RayBot are approximated as an interconnection of a finite number of bodies. A BAUV simulation and 3D visualization platform (Figures 7 and 8) has also been implemented based on the proposed multi-body modeling approach.

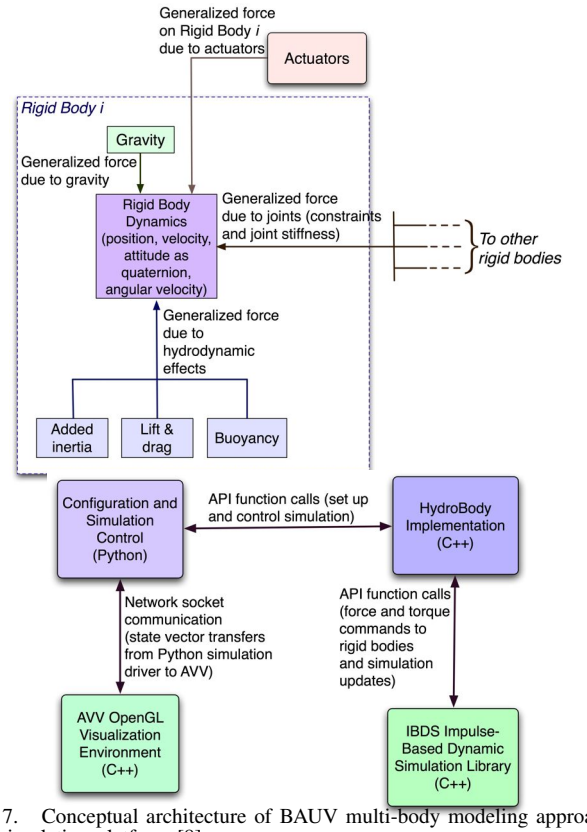

Fig. 7. Conceptual architecture of BAUV multi-body modeling approach and simulation platform [8].

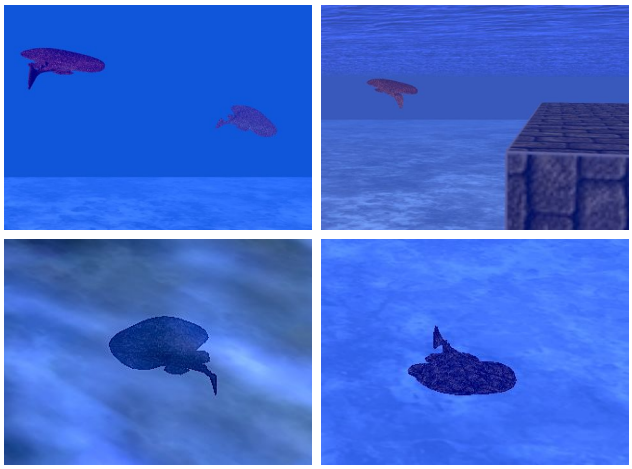

Fig. 8. Screenshots from AVV for BAUV simulation. Note actuation of tail, body disc, and pelvic fins. Note also support for simultaneous simulation of multiple BAUVs and for obstacles in environment.

IV. RayBot Design and Implementation

The experimental development of the RayBot3 BAUV proceeded through three hardware versions: RayBot 3.1, RayBot 3.2, and RayBot 3.3. The actuation mechanisms of the RayBot prototypes followed this design arc: external tendons driven by central servo (RayBot 3.1) → external tendons with retinaculae driven by central servo (RayBot 3.2) → internal fin-shear mechanism driven by central servo (RayBot 3.3). While the RayBot hardware prototypes presented in this paper are powered by servo motors, preliminary experimental testing and trade-off analysis have been performed for various alternative actuators including hydraulics, linear piezoelectric motors, linear magnetic motors, magnetic switches, and Nitinol-based shape memory alloy. An ideal actuator for

RayBot should be distributed, efficient, silent, compact, and inexpensive. Further evaluation of these alternative actuators and integration into RayBot is planned for future effort.

RayBot 3.1 and RayBot 3.2: RayBot prototypes 3.1 and 3.2 utilized tendon-based actuation of the tail. The silicone caudal fin, attached to the rigid housing, was shaped roughly like that of an electric ray (see Figure 6), and was flexible, having a Shore A hardness of 10 (silicone-based polymer) similar to that found in fish bodies. The caudal fin in RayBot 3.1 is controlled by two contra-lateral cables (polystyrene cables operating as tendons) driven by a coreless servo motor. Vehicle pitch and roll are controlled by two pectoral fin servos with leading-edge actuated in pitch by servos. The self-propelled RayBot 3.1 achieved a swimming speed of 5.3 cm s^{-1} with a tailbeat frequency of 2.5 Hz. Motions of the biomimetic tail compared well, qualitatively, to that of the live swimming electric ray. RayBot 3.2 utilized the same biologically inspired caudal fin mechanism as RayBot 3.1 and the tendon-based transmission system was improved by adding guides, or what are called retinaculae in vertebrate tendon systems, that prevent the tendons from bowstringing during tail bending (Figure 9). The retinaculae create a more mechanically efficient transmission system, giving more curvature per angular unit of servo displacement, resulting in a 3x improvement in swimming speed over RayBot 3.1, with top forward speeds of 16 cm s^{-1}. With RayBot 3.2, we conducted an empirical investigation (using data digitized from an overhead video capture system) to examine the relationship between tail-beat frequency, tail-beat amplitude, and speed, and to compare these relationships with simulations. Comparisons between simulation results and experimentally observed data for RayBot 3.2 are illustrated in Figure 10.

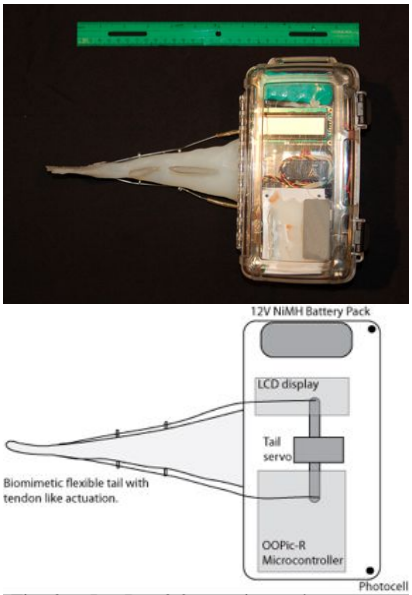

Fig. 9. RayBot 3.2 experimental prototype.

RayBot 3.3: The third RayBot prototype (Figure 11) addressed improvement of the biologically-inspired transmission system as well as implementation of an AUV with the complex body shape of a real electric ray. For inspiration, we turned to the fin skeleton of teleost fishes, which have, in each fin ray, a split skeletal system, attached at the distal end, driven proximally by paired muscles that create an offset between hemitrichts. Fin rays thus actuated are used for propulsion and for postural (shape) control of

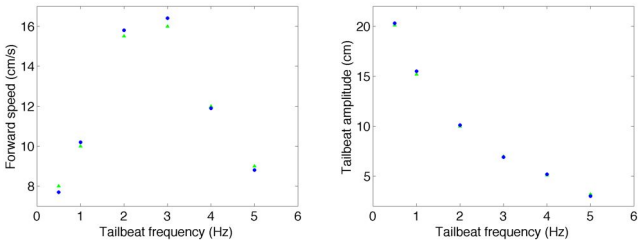

Fig. 10. Comparison of experimental vs. simulation results for forward swimming performance of RayBot 3.2. Left: Tailbeat frequency vs. tailbeat amplitude (Green triangles: experiment, Blue circles: simulation); Right: Tailbeat frequency vs. maximum cruising forward speed (Green triangles: experiment, Blue circles: simulation).

non-propulsive fins, thus, suggesting a functionally versatile actuation mechanism. Fish fins contain a series of rays with each ray composed of two hemitrichs. Each hemitrich is independently actuated by muscles via tendons. The offset or shear between the hemitrichs creates bending because the tips are joined. For our RayBot fins, we use a mechanically analogous system, with the hemitrichs driven by a servo motor. The fin-ray-based mechanism is implemented in RayBot 3.3 by a fin-shear actuator (FSA – see Figure 13). A single FSA can be driven by a single servo motor. A rack-and-pinion drives the offset of one side of the paired fin back and forth relative to the other side, which is anchored to the non-moving parts of the servo. This linear offset creates oscillating flexures. While the basic concept of the fin-shear actuation mechanism has been addressed previously in the literature [21,22], our design here provides a general mechanism which is scalable to large sizes. Furthermore, the FSA design here provides a moment generator for the whole body. The FSA design is particularly attractive since it centralizes motors resulting in a simple, mechanically robust, light transmission system.

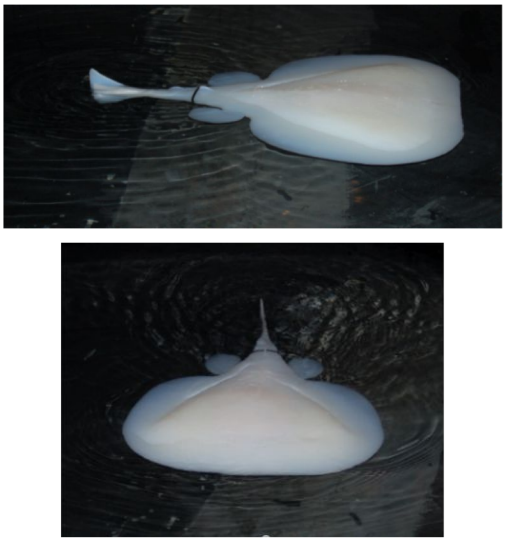

Fig. 11. RayBot 3.3 experimental prototype.

RayBot 3.3 is housed in a biomimetic body (Figures 11 and 12) based on a model constructed from a real electric ray. To build a body for RayBot that was accurate biologically, a large electric ray, *Torpedo nobiliana*, with a 50 cm disk span was cast in plaster. While different from the electric ray we have used for biological studies in this effort, this species of electric ray, *Torpedo nobiliana*, was chosen primarily for its size, 75 cm long x 50 cm wide, which was large enough to contain the necessary mechanical and electrical elements

but remain a man-portable device. Using a two-piece plaster mold of the electric ray, a cast of the ray was made out of a flexible, silicone based polymer. While the initial intent was to use this mold to build the body for RayBot 3.3, it was noted, upon examining the first cast, that there were multiple body asymmetries caused by the movement of the viscera during molding. Not wanting to make these asymmetries part of our final design, we decided to use the cast as the basis for creating a computer-based cast. Precise measurements of the cast were made and digitally rendered. The final 3D graphics cast preserves the proportions of the biological target while enforcing left-right symmetry, smooth surfaces, and regular transitions. The computer model can be resized to produce rays of different scales. The surface coordinates were then transferred from the digital 3D model to the format used by our 3-axis CNC milling machine. The payload and the fin-based actuator system were included in the mold; silicone was poured into the mold, thus embedding the payload and the actuator within the unitary body. The final cast was trimmed to remove excess fringe material.

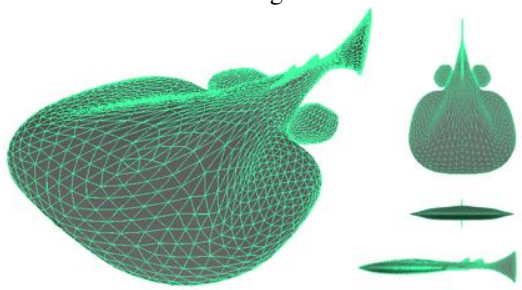

Fig. 12. Design of biomimetic body of RayBot 3.3.

The final casted ray is 75 cm long x 50 cm wide, with a maximal height of 15cm at the tip of the caudal fin and disc height of 9 cm. It weighs 5.5 kg, and is easily carried by a single person. Without ballast or payload, the swimming RayBot 3.3 is slightly buoyant, resting mostly under the water's surface with the very top portion of the body disc exposed. (Figure 11). The electronics contained is completely submerged and our waterproofing system works reliably. As in RayBot 3.2, RayBot 3.3 has a performance peak in the middle of its tailbeat frequency range (see Figure 14), irrespective of the servo driving amplitude. The red and blue dots represent different servo amplitudes, $\pm 22.5^o$ and $\pm 45^o$. The performance peak occurs because the tailbeat amplitude decreases with increasing tailbeat frequency (middle graph of Figure 14). Note that the tailbeat amplitudes between the two servo amplitudes do not differ appreciably; thus speed differences occur because of hydrodynamic effects upstream from the trail edge. While the top speed of just over 10 cm s^{-1} is intermediate between top speeds of RayBot 3.1 and 3.2, RayBot 3.3 is more massive and with more wetted surface area. To test gliding and drag, we programmed RayBot 3.3 to accelerate from rest and then glide without bending its tail after 14 tailbeats (see Figure 14). Over the acceleration period, average acceleration is 0.93 cm s^2; average acceleration during the glide phase is -0.35 cm s^2. Knowing the mass of the body to be 5.5 kg, we calculated drag on the decelerating body as approximately 0.02 N. From calculation of the projected surface area of RayBot 3.3, we could compute the drag characteristics; the coefficient of drag (projected area) was estimated to be 0.032, a value well within the range for streamlined bodies.

The fin-shear mechanism that currently actuates the RayBot tail is being extended in on-going effort to the pelvic fins and to the body perimeter. A simulation-based trade-off analysis was performed of the number of points that need to be actuated in the RayBot's body perimeter taking into account possible maneuverability, mechanical complexity, power requirement, and cost. While a distributed muscle-type actuator could potentially enable continuous body perimeter actuation, the fin-shear mechanism considered here provides effective single-axis actuation so that reduction of the number of points on the body perimeter needed to be actuated would provide improved mechanical simplicity as well as mechanical robustness leading to potential longevity of the BAUV in operation. It was found that dorsoventral actuation of five points on the body perimeter (Figure 15) provides an effective design trade-off point. Actuation of 5 points enables efficient control of roll (through actuation of lateral 4 points) as well as diving (through control of frontal surface area by actuation of frontal 3 points) The fin-shear actuation mechanism provides efficient actuation of these body perimeter points.

For the full 6DOF modeling of the biomimetic RayBot 3.3 in simulation, 9 bodies and 9 hinge joints are used. The body disc is decomposed into a central rigid part and four separately actuated planes in the periphery (corresponding to 4 hinge joints; physically, as shown in Figure 15, this is realized through 5 actuated points at the circumference connected as in a wheel spoke with central points which are the roots of fin-shear actuators). The pelvic fins are separate bodies connected to the central body through hinge joints. The tail is composed of two bodies connected to each other and to the central body through hinge joints. Finally, an additional hinge joint allows bending (nominally with respect to horizontal plane) between the central body plane and the tail bodies (this is primarily exercised in diving behavior of the electric ray). Sets of configuration files and Python configuration scripts were developed for representative live adult and neonate electric ray specimens as well as of the RayBot prototype versions 3.1, 3.2, and 3.3. Simulation studies were performed on each of the implemented models to attain a qualitative and quantitative understanding of electric ray swimming mechanisms and to provide data for fin design and trade-off analysis. A sample simulation of acceleration and deceleration of the RayBot 3.3 is shown in Figure 16 wherein the tailbeat ferquency was set to 5 rad/s until 12 seconds after which the tail was held steady.

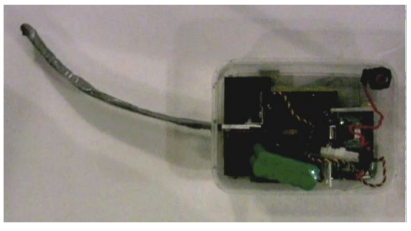

Fig. 13. Fin-shear actuation mechanism.

Auto-Pilot System: A custom-designed compact BAUV auto-pilot hardware (Figure 17) has been developed to facilitate implementation and testing of real-time autonomous navigation and control laws for the RayBot. The auto-pilot hardware has been specifically designed taking into account the computational requirements of a BUAV as well as the size, power, and weight constraints. The onboard microprocessor provides several I/O channels and PWM outputs and can, therefore, handle interfacing to the sensors and actuators required to control the RayBot. The supported sensor suite

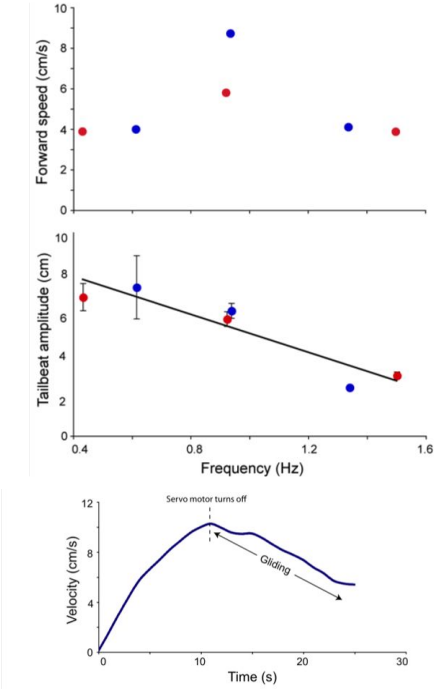

Fig. 14. RayBot 3.3 swimming and gliding performance. The red and blue dots represent different servo amplitudes, $\pm 22.5^o$ and $\pm 45^o$

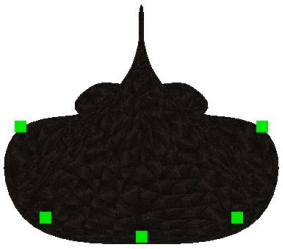

Fig. 15. Actuation of the body perimeter at 5 points.

includes a three-axis inertial measurement unit (IMU), a three axis magnetometer, static and dynamic pressure sensors, acoustic sensors (sonars), IR sensors, and a leak sensor.

V. Concluding Remarks

The development of a novel BAUV inspired by the electric ray was addressed. As part of the effort, an experimental self-propelled hardware prototype of the RayBot BAUV was implemented. A 6DOF modeling technique was also developed using an impulse-based multi-body approach for a generic BAUV and a simulation and visualization platform was also implemented and validated against experimental data both from the various RayBot prototypes as well as from live juvenile electric rays. Integration of further actuation mechanisms into the RayBot and autonomous navigation capabilities using the developed auto-pilot system are being addressed in on-going studies.

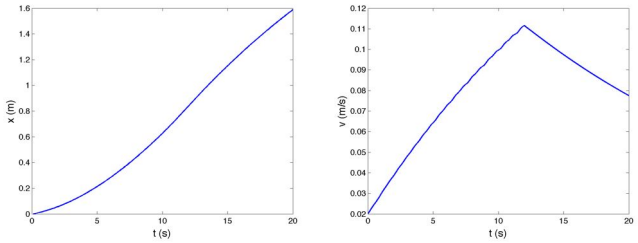

Fig. 16. Sample acceleration and deceleration profiles for forward swimming performance simulation of RayBot 3.3.

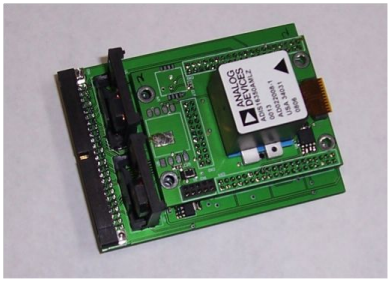

Fig. 17. Custom-designed auto-pilot system for robotic fish.

References

[1] B. Fletcher, "UUV master plan: a vision for navy UUV development," in *Proc. of the OCEANS 2000 MTS/IEEE Conf. and Exhibition*, Providence, RI, Sept. 2000, pp. 65–71.

[2] G. Griffiths, *Technology and Applications of Autonomous Underwater Vehicles*. CRC Press, 2002.

[3] J. D. Lambert, P. Picarello, and J. E. Manley, "Development of UUV standards, an emerging trend," in *Proc. of the OCEANS 2006 MTS/IEEE Conf. and Exhibition*, Boston, MA, Sept. 2006, pp. 1–5.

[4] M. S. Triantafyllou, A. H. Techet, and F. S. Hover, "Review of experimental work in biomimetic foils," *IEEE Journal of Oceanic Engineering*, vol. 29, no. 3, pp. 585–594, July 2004.

[5] P. R. Bandyopadhyay, "Trends in biorobotic autonomous undersea vehicles," *IEEE Journal of Oceanic Engineering*, vol. 30, no. 1, pp. 109–139, Jan. 2005.

[6] M. Sfakiotakis, D. M. Lane, and J. B. C. Davies, "Review of fish swimming modes for aquatic locomotion," *IEEE Journal of Oceanic Engineering*, vol. 24, no. 2, pp. 237–252, April 1999.

[7] J. C. Carrier, J. A. Musick, and M. R. Heithaus, *Biology of Sharks and Their Relatives*. CRC Press, 2004.

[8] P. Krishnamurthy, F. Khorrami, J. de Leeuw, M. E. Porter, K. Livingston, J. H. Long, Jr., "A multi-body approach for 6DOF modeling of biomimetic autonomous underwater vehicles with simulation and experimental results," in *Proc. of the IEEE Multi-Conf. on Systems and Control*, (St. Petersburg, Russia), July 2009.

[9] J. S. Nelson, *Fishes of the World*. John Wiley and Sons, 1994.

[10] J. T. Schaefer and A. P. Summers, "Batoid wing skeletal structure: novel morphologies, mechanical implications and phylogenetic patterns," *Journal of Morphology*, vol. 265, pp. 298–313, 2005.

[11] R. Froese and D. Pauly, "Fishbase," 2007, world Wide Web electronic publication. http://www.fishbase.org, version (11/2007).

[12] M. J. Lighthill, "Note on the swimming of slender fish," *Journal of Fluid Mechanics*, vol. 9, no. 2, pp. 305–317, 1960.

[13] T. Y. Wu, "Swimming of a waving plate," *Journal of Fluid Mechanics*, vol. 10, no. 3, pp. 321–344, 1961.

[14] K. A. Harper, M. D. Berkemeier, and S. Grace, "Modeling the dynamics of spring-driven oscillating-foil propulsion," *IEEE Journal of Oceanic Engineering*, vol. 23, no. 3, pp. 285–296, July 1998.

[15] J. E. Colgate and K. M. Lynch, "Mechanics and control of swimming: A review," *IEEE Journal of Oceanic Engineering*, vol. 29, no. 3, pp. 660–673, July 2004.

[16] L. Liu, J. Yu, and L. Wang, "Dynamic modeling of three-dimensional swimming for biomimetic robotic fish," in *Proc. of the IEEE International Conf. on Intelligent Robots and Systems*, Beijing, China, Oct. 2006, pp. 3916–3921.

[17] J. Yu, L. Liu, and M. Tan, "Dynamic modeling of multi-link swimming robot capable of 3-d motion," in *Proc. of the IEEE International Conf. on Mechatronics and Automation*, Harbin, China, Aug. 2007, pp. 1322–1327.

[18] D. Adkins and Y. Y. Yan, "CFD simulation of fish-like body moving in viscous liquid," *Journal of Bionic Engineering*, vol. 3, no. 3, pp. 147–153, Sep. 2006.

[19] J. Bender and A. Schmitt, "Fast dynamic simulation of multi-body systems using impulses," in *Proc. of the Virtual Reality Interactions and Physical Simulations*, Madrid, Spain, Nov. 2006.

[20] J. Bender, "Impulse-based dynamic simulation in linear time," *Journal of Computer Animation and Virtual Worlds*, 2007.

[21] J. L. Tangorra, S. N. Davidson, I. W. Hunter, P. G. A. Madden, G. V. Lauder, H. Dong, M. Bozkurttas, and R. Mittal, "The development of a biologically inspired propulsor for unmanned underwater vehicles," *IEEE Journal of Oceanic Engineering*, vol. 32, no. 3, pp. 533–550, July 2007.

[22] S. Alben, P. G. Madden, and G. V. Lauder, "The mechanics of active fin-shape control in ray-finned fishes," *Journal of the Royal Society Interface*, vol. 4, pp. 243–256, 2007.